Hindawi
Mathematical Problems in Engineering
Volume 2017, Article ID 2409179, 11 pages
https://doi.org/10.1155/2017/2409179

Research Article

A Bearingless Induction Motor Direct Torque Control and Suspension Force Control Based on Sliding Mode Variable Structure

Zebin Yang,[1] Lin Chen,[1] Xiaodong Sun,[2] Weiming Sun,[1] and Dan Zhang[1]

[1]*School of Electrical and Information Engineering, Jiangsu University, Zhenjiang 212013, China*
[2]*Automotive Engineering Research Institute, Jiangsu University, Zhenjiang 212013, China*

Correspondence should be addressed to Xiaodong Sun; xdsun@ujs.edu.cn

Received 31 March 2017; Accepted 14 June 2017; Published 1 August 2017

Academic Editor: Jun M. Wang

Aiming at the problems of the large torque ripple and unstable suspension performance in traditional direct torque control (DTC) for a bearingless induction motor (BIM), a new method of DTC is proposed based on sliding mode variable structure (SMVS). The sliding mode switching surface of the torque and flux linkage controller are constructed by torque error and flux error, and the exponential reaching law is used to design the SMVS direct torque controller. On the basis of the radial suspension force mathematical model of the BIM, a radial suspension force closed-loop control method is proposed by utilizing the inverse system theory and SMVS. The simulation models of traditional DTC and the new DTC method based on SMVS of the BIM are set up in the MATLAB/Simulink toolbox. On this basis, the experiments are carried out. Simulation and experiment results showed that the stable suspension operation of the BIM can be achieved with small torque ripple and flux ripple. Besides, the dynamic response and suspension performance of the motor are improved by the proposed method.

1. Introduction

Bearingless motors inherited the characteristics of the traditional magnetic bearing motors, such as being without lubrication, having no wear, and having no mechanical noise. Compared with the traditional magnetic bearing motor, the space utilization rate, electromagnetic efficiency, and other aspects have been improved. It is of great significance to the development of the field of the biochemical medicine and industrial field such as the heart blood pump, the turbo molecular pump, and the high speed flywheel energy storage system [1, 2]. The levitation windings of bearingless motors, breaking the balance of the original state of the air gap magnetic field, changing the distribution of the air gap magnetic field, and producing the Maxwell force which have an effect on the rotor were to realize the stable suspension. Many scholars at home and abroad have studied the bearingless permanent magnet motor. However, the bearingless induction motor (BIM) has the advantages of low loss, low cost, simple structure, and withstanding high temperature, and it is easy to realize the open-loop speed control by the voltage source inverter, which people are increasingly concerned with [3].

The BIM is a strongly coupled nonlinear system. In order to realize the decoupling between the radial suspension force and the torque, the rotor flux oriented vector control is introduced into the BIM in [4]. However, the use of the rotor flux instead of the air gap flux in this method has bad influence on the rotor stable suspension. Reference [5] overcame the limitation of rotor flux orientation, introduced the air gap flux oriented of the BIM, and deduced the suspension force expression of the air gap flux oriented control, but the control algorithm is much more complicated and highly nonlinear, and the torque response will be instable, which makes the application of this method limited.

Direct torque control (DTC) is another way of AC speed regulation after field oriented vector control. The method is simple and does not need the complex vector transform and current control, which improves the dynamic response of the system. From the retrieved papers, there are not many

literatures researching on the DTC of bearingless motor. The DTC is introduced into the bearingless permanent magnet synchronous motor and the bearingless permanent magnet slice motor in [6, 7]. The DTC is applied to the BIM in [8, 9] and the DTC based on space vector pulse width modulation is proposed. The experimental results showed that the method can realize the stable suspension of the motor. However, the traditional DTC has the problems of high torque ripple and nonfixed switching frequency. Because the stator flux estimation directly affects the performance of DTC, a large number of papers have been studied on the stator flux estimation [10–12]. Some papers committed to improving the structure of the controller [13–16], but these controllers have increased the complexity of the system, which make the control system of the BIM more complicated and influence the motor stable suspension operation.

In order to reduce the torque ripple and improve the performance of the traditional DTC of the BIM, sliding mode variable structure (SMVS) control is introduced to the DTC system. Two hysteresis controllers in the traditional DTC are replaced by the sliding mode controller. The switching table is no longer used to select the space voltage vector; instead, the voltage vectors of the two-phase static coordinate system are output by the sliding mode controller, which is constructed according to the torque error and flux linkage error. The choice of inverter switching value based on space voltage pulse width modulation (SVPWM) reduces the torque ripple fundamentally.

The BIM control system includes torque control and suspension force control. For the part of suspension force control, the traditional method is by detecting the radial displacement of the rotor, and the given value of suspension force is obtained by the PID modulation, which can realize the closed-loop control of the suspension force [17]. The method is relevant to air gap flux identification, and its dynamic response and the anti-interference performance are not good. To overcome this problem, the SMVS suspension force control method based on inverse system is proposed. On the basis of the radial suspension force mathematical model of the BIM, the reversibility of the inverse system is analyzed; the SMVS control is introduced into the inverse system and realized suspension force control. The BIM DTC and suspension force control system based on SMVS are built in MATLAB/Simulink toolbox. The dynamic performance of the torque response and the rotor suspension performance are compared and analyzed for two cases that are based on traditional DTC and SMVS-DTC, respectively. On this basis, the experiments were carried out. Simulation and experiment results showed that the torque ripple has greatly reduced and the performance of the rotor suspension is improved.

2. Sliding Mode Variable Structure Direct Torque Control of the BIM

2.1. Principle of SMVS. SMVS control is a special kind of nonlinear control method, which is a kind of control strategy of variable structure control system. The difference between this control strategy and the traditional control strategy is that the control is not continuous. It is a kind of switching characteristic that makes the system structure change with time. The control strategy makes the system pass through the prescribed state locus back and forth in high frequency and small amplitude. Because the state locus can be designed, and not related to the system parameters and outside disturbance, it has a strong robustness [18].

Sliding mode variable structure control has three basic problems: firstly, the sliding mode should exist; secondly, the reach-ability condition should be satisfied; finally, the stability of the sliding mode should be analyzed [19–21].

2.2. Design of SMVS-DTC Controller. SMVS controller is used to replace the traditional hysteresis comparators. The torque winding reference voltage vector should be calculated by torque error and flux error, and thus the controller includes flux controller and torque controller.

The mathematical model of the BIM in the two-phase stationary α-β coordinate system and with the torque winding stator current and stator flux as state variables is as follows:

$$\begin{aligned}
\frac{d}{dt}i_{1s\alpha} &= -\frac{1}{\sigma\left(\dfrac{R_{1s}}{L_{1s}}+\dfrac{R_{1r}}{L_{1r}}\right)}i_{1s\alpha} - \omega_r i_{1s\beta} \\
&\quad + \frac{R_{1r}}{\sigma L_{1s}L_{1r}}\psi_{1s\alpha} + \frac{\omega_r}{\sigma L_{1s}}\psi_{1s\beta} + \frac{1}{\sigma L_{1s}}u_{1s\alpha}, \\
\frac{d}{dt}i_{1s\beta} &= -\frac{1}{\sigma\left(\dfrac{R_{1s}}{L_{1s}}+\dfrac{R_{1r}}{L_{1r}}\right)}i_{1s\beta} + \omega_r i_{1s\alpha} \\
&\quad + \frac{R_{1r}}{\sigma L_{1s}L_{1r}}\psi_{1s\beta} - \frac{\omega_r}{\sigma L_{1s}}\psi_{1s\alpha} + \frac{1}{\sigma L_{1s}}u_{1s\beta}, \\
\frac{d}{dt}\psi_{1s\alpha} &= u_{1s\alpha} - R_{1s}i_{1s\alpha}, \\
\frac{d}{dt}\psi_{1s\beta} &= u_{1s\beta} - R_{1s}i_{1s\beta},
\end{aligned} \tag{1}$$

where $\sigma = 1 - L_{1m}^2/L_{1s}L_{1r}$; $i_{1s\alpha}$ and $i_{1s\beta}$, respectively, represent two components of the torque winding stator current and rotor current in coordinate system. $\psi_{1r\alpha}$ and $\psi_{1r\beta}$, respectively, represent two components of the torque winding stator flux and rotor flux in coordinate system. L_{1s} and L_{1r} are stator and rotor self-inductance of torque winding. R_{1s} and R_{1r} are stator and rotor resistance of torque winding; L_{1m} is mutual inductance between stator and rotor of torque winding. $u_{1s\alpha}$ and $u_{1s\beta}$, respectively, represent two components of the torque winding stator voltage and rotor voltage in coordinate system. ω_r is the rotor angular velocity.

The electromagnetic torque equation of the BIM is as follows:

$$T_e = \frac{3}{2}P_1\left(\psi_{1s\alpha}i_{1s\beta} - \psi_{1s\beta}i_{1s\alpha}\right), \tag{2}$$

where P_1 is the number of the pole-pairs of torque winding.

The voltage-current model is used to estimate the stator flux of the torque winding in the two-phase stationary coordinate system (α-β).

$$\begin{aligned}\psi_{1s\alpha} &= \int \left(u_{1s\alpha} - R_{1s} i_{1s\alpha}\right) dt,\\ \psi_{1s\beta} &= \int \left(u_{1s\beta} - R_{1s} i_{1s\beta}\right) dt.\end{aligned} \tag{3}$$

In order to track the desired trajectory of the torque and flux, the sliding mode switching surface is selected as follows:

$$\begin{aligned}S_1 &= T_e^* - T_e,\\ S_2 &= \psi_{1s}^{2*} - \psi_{1s}^2,\\ S &= \begin{bmatrix} S_1 & S_2 \end{bmatrix}^T,\end{aligned} \tag{4}$$

where T_e^* and ψ_{1s}^{2*} are the given values of torque and the square of flux. T_e and ψ_{1s}^2 are the calculated values of torque and the square of flux.

To make the system have a good dynamic performance, the reaching law is selected as the exponential reaching law:

$$\dot{S} = -\varepsilon \operatorname{sgn} S - KS, \tag{5}$$

where ε and K are positive constants. When the value of ε is very small and the value of K is great, the speed of the reaching law away from the switching surface is fast and near the switching surface is slow. This can effectively reduce the chattering and shorten the transition time [22].

Calculating the derivation of S_1 and S_2,

$$\begin{aligned}\dot{S}_1 = &-\frac{3}{2} \cdot P_1 \left[\frac{1}{\sigma \left(R_{1s}/L_{1s} + R_{1r}/L_{1r}\right)} \left(\psi_{1s\beta} i_{1s\alpha} - \psi_{1s\alpha} i_{1s\beta}\right) \right.\\ &+ \omega_r \left(\psi_{1s\alpha} i_{1s\alpha} + \psi_{1s\beta} i_{1s\beta}\right) - \frac{\omega_r}{\sigma L_{1s}} \psi_{1s}^2\\ &\left. + \left(i_{1s\beta} - \frac{\psi_{1s\beta}}{\sigma L_{1s}}\right) u_{1s\alpha} - \left(i_{1s\alpha} - \frac{\psi_{1s\beta}}{\sigma L_{1s}}\right) u_{1s\beta} \right] = C_1\\ &+ D_1 u,\end{aligned} \tag{6}$$

where $\psi_{1s}^2 = \psi_{1s\alpha}^2 + \psi_{1s\beta}^2$.

$$\begin{aligned}\dot{S}_2 = &-2\psi_{1s\alpha} u_{1s\alpha} - 2\psi_{1s\beta} u_{1s\beta}\\ &+ 2R_s \left(\psi_{1s\alpha} i_{1s\alpha} + \psi_{1s\beta} i_{1s\beta}\right) = C_2 + D_2 u,\end{aligned} \tag{7}$$

in which C_1, D_1, C_2, D_2, and u are as follows:

$$\begin{aligned}C_1 = &-\frac{3}{2} P_1 \left[\frac{1}{\sigma \left(\dfrac{R_{1s}}{L_{1s}} + \dfrac{R_{1r}}{L_{1r}}\right)} \left(\psi_{1s\beta} i_{1s\alpha} - \psi_{1s\alpha} i_{1s\beta}\right) \right.\\ &\left. + \omega_r \left(\psi_{1s\alpha} i_{1s\alpha} + \psi_{1s\beta} i_{1s\beta}\right) - \frac{\omega_r}{\sigma L_{1s}} \psi_{1s}^2 \right],\\ D_1 = &\left[-\frac{3}{2} P_1 \left(i_{1s\beta} - \frac{\psi_{1s\beta}}{\sigma L_{1s}}\right) \quad \frac{3}{2} P_1 \left(i_{1s\alpha} - \frac{\psi_{1s\alpha}}{\sigma L_{1s}}\right) \right],\\ C_2 = &\, 2R_s \left(\psi_{1s\alpha} i_{1s\alpha} + \psi_{1s\beta} i_{1s\beta}\right),\\ D_2 = &\left[-2\psi_{1s\alpha} \quad -2\psi_{1s\beta} \right],\\ u = &\left[u_{1s\alpha} \quad u_{1s\beta} \right]^T.\end{aligned} \tag{8}$$

Combining (5) and (6) one can obtain

$$\dot{S} = \begin{bmatrix} \dot{S}_1 \\ \dot{S}_2 \end{bmatrix} = \begin{bmatrix} C_1 \\ C_2 \end{bmatrix} + \begin{bmatrix} D_1 \\ D_2 \end{bmatrix} \begin{bmatrix} u_{1s\alpha} \\ u_{1s\beta} \end{bmatrix}. \tag{9}$$

Substituting (4) into (7) one can obtain the controller formula:

$$u = -D^{-1} \begin{bmatrix} C_1 + \varepsilon_1 \operatorname{sgn}\left(S_1\right) + K_1 S_1 \\ C_2 + \varepsilon_2 \operatorname{sgn}\left(S_2\right) + K_2 S_2 \end{bmatrix} \tag{10}$$

and $D^{-1} = \left[\begin{smallmatrix} d_1 & d_2 \\ d_3 & d_4 \end{smallmatrix} \right]$, where

$$\begin{aligned}d_1 &= \frac{-2\psi_{1s\beta}}{3p_1 \left(\psi_{1s\beta} i_{1s\beta} + \psi_{1s\alpha} i_{1s\alpha}\right) - 3p_1 \left(\psi_{1s\beta}^2 + \psi_{1s\alpha}^2\right)/\sigma L_{1s}};\\ d_2 &= \frac{-1.5p_1 \left(i_{1s\alpha} - \psi_{1s\alpha}/\sigma L_{1s}\right)}{3p_1 \left(\psi_{1s\beta} i_{1s\beta} + \psi_{1s\alpha} i_{1s\alpha}\right) - 3p_1 \left(\psi_{1s\beta}^2 + \psi_{1s\alpha}^2\right)/\sigma L_{1s}};\\ d_3 &= \frac{2\psi_{1s\alpha}}{3p_1 \left(\psi_{1s\beta} i_{1s\beta} + \psi_{1s\alpha} i_{1s\alpha}\right) - 3p_1 \left(\psi_{1s\beta}^2 + \psi_{1s\alpha}^2\right)/\sigma L_{1s}};\\ d_4 &= \frac{-1.5p_1 \left(i_{1s\beta} - \psi_{1s\beta}/\sigma L_{1s}\right)}{3p_1 \left(\psi_{1s\beta} i_{1s\beta} + \psi_{1s\alpha} i_{1s\alpha}\right) - 3p_1 \left(\psi_{1s\beta}^2 + \psi_{1s\alpha}^2\right)/\sigma L_{1s}}.\end{aligned} \tag{11}$$

2.3. Analyses of the Reach-Ability Condition of the Sliding Mode. If the sliding mode exists, the moving point beyond the switching surface will reach the switching surface in finite

time and the sliding mode motion is stable. The following reach-ability condition is satisfied:

$$\lim_{S\to 0^+} \dot{S} < 0, \qquad \lim_{S\to 0^-} \dot{S} > 0. \tag{12}$$

The global reach-condition is $S\dot{S} < 0$. From the exponential reaching law, it can be obtained that

$$S\dot{S} = S\left(-\varepsilon \operatorname{sgn} S - KS\right) = -\varepsilon |S| - KS^2. \tag{13}$$

Because ε and K are positive constant, $S\dot{S} < 0$. The sliding mode satisfies the reach-ability condition.

2.4. Analyses of the Stability of SMVS-DTC Controller. Selecting Lyapunov function: $V = SS^T/2$, the derivation of it can be calculated:

$$\begin{aligned} \dot{V} &= \begin{bmatrix} S_1 & S_2 \end{bmatrix} \begin{bmatrix} -\varepsilon_1 \operatorname{sgn} S_1 - K_1 S_1 \\ -\varepsilon_2 \operatorname{sgn} S_2 - K_2 S_2 \end{bmatrix} \\ &= -S_1\left(\varepsilon_1 \operatorname{sgn} S_1 + K_1 S_1\right) - S_2\left(\varepsilon_2 \operatorname{sgn} S_2 + K_2 S_2\right) \\ &= -\varepsilon_1 |S_1| - K_1 S_1^2 - \varepsilon_2 |S_2| - K_2 S_2^2, \end{aligned} \tag{14}$$

in which ε_1, K_1, ε_2, and K_2 are positive constant, so it can be obtained that

$$\dot{V} = -\varepsilon_1 |S_1| - K_1 S_1^2 - \varepsilon_2 |S_2| - K_2 S_2^2 < 0. \tag{15}$$

It can be concluded that this SMVS-DTC controller satisfies the stability conditions.

3. SMVS Suspension Force Control of the BIM

3.1. Radial Suspension Force Mathematical Model of the BIM. According to the relationship between the suspension force and the suspension winding stator current of the BIM in the two-phase stationary coordinate system (α-β) [23],

$$\begin{aligned} F_x &= K_m\left(i_{2s\alpha}\psi_{1\alpha} + i_{2s\beta}\psi_{1\beta}\right), \\ F_y &= K_m\left(i_{2s\beta}\psi_{1\alpha} - i_{2s\alpha}\psi_{1\beta}\right), \end{aligned} \tag{16}$$

where $K_m = \pi P_1 P_2 L_{2m}/18\mu_0 lrW_1W_2$. P_1 and P_2 are the numbers of pole-pairs of torque winding and suspension winding, respectively. $\psi_{1\alpha}$ and $\psi_{1\beta}$ are the component of air gap flux in α-β axis, respectively. F_x and F_y are the suspension force of radial x and y. L_{2m} is the mutual inductance between stator and rotor of suspension winding. μ_0 is the permeability of vacuum. l is the effective length of the rotor. r is the outside diameter of rotor. W_1 and W_2 are the torque winding turns and suspension winding turns.

When the rotor deviates from the center of the motor stator, it will cause the motor flux distribution. Then the Maxwell force is not zero, and the direction of its action and the direction of the rotor eccentricity are consistent, pointing to the direction of minimum air gap; it is called unbalanced magnetic force and is showed as

$$\begin{aligned} F_{sx} &= k_s x, \\ F_{sy} &= k_s y, \end{aligned} \tag{17}$$

where $k_s = k(\pi rlB_1^2/2\mu_0 g_0)$ and F_{sx} and F_{sy} are the unbalanced magnetic force in the direction of x and y, respectively. x and y are the displacement in the direction of x and y, respectively, and g_0 is the air gap length.

The motion equations of the rotor are expressed as

$$\begin{aligned} m\ddot{x} &= F_x - F_{sx}, \\ m\ddot{y} &= F_y - F_{sy} - mg, \end{aligned} \tag{18}$$

where m is the mass of the rotor and g is the gravity acceleration. By (16)–(18), it can be obtained that

$$\begin{aligned} \ddot{x} &= \frac{\left[K_m\left(i_{2s\alpha}\psi_{1\alpha} + i_{2s\beta}\psi_{1\beta}\right) - k_s x\right]}{m}, \\ \ddot{y} &= \frac{\left[K_m\left(i_{2s\beta}\psi_{1\alpha} - i_{2s\alpha}\psi_{1\beta}\right) - k_s y - mg\right]}{m}. \end{aligned} \tag{19}$$

3.2. SMVS Radial Suspension Force Control of the BIM Based on Inverse System. The basic principle of inverse system method is to compensate the controlled object as a system with a linear transfer relationship by using the inverse system of the controlled object, then, to synthesize the system according to the linear system theory, and to realize the decoupling in nonlinear systems [24, 25].

Theorem 1. *For a system of p dimensional input, $u(t) = (u_1, u_2, \ldots, u_p)^T$, and, for q dimensional output, $y(t) = (y_1, y_2, \ldots, y_q)^T$, with a set of initial states $x(t_0) = x_0$, and it can be expressed as the following state equation:*

$$\begin{aligned} \dot{x} &= f(x,u), \\ y &= h(x,u), \\ x(t_0) &= x_0. \end{aligned} \tag{20}$$

The necessary and sufficient condition for the system to be reversible in the neighborhood of (x_0, u_0) has vector relative order $\alpha = (\alpha_1, \alpha_2, \ldots, \alpha_q)^T$ in this neighborhood.

Select the state variables in (19).

$$X = \begin{bmatrix} x_1 & x_2 & x_3 & x_4 \end{bmatrix}^T = \begin{bmatrix} x & y & \dot{x} & \dot{y} \end{bmatrix}^T. \tag{21}$$

The input variable is

$$U = \begin{bmatrix} u_1 & u_2 \end{bmatrix}^T = \begin{bmatrix} i_{2s\alpha} & i_{2s\beta} \end{bmatrix}^T. \tag{22}$$

The output variable is

$$Y = \begin{bmatrix} y_1 & y_2 \end{bmatrix}^T = \begin{bmatrix} x & y \end{bmatrix}^T. \tag{23}$$

The state equation of the composite controlled object is obtained by (19) and(21):

$$\begin{aligned}
\dot{x}_1 &= x_3,\\
\dot{x}_2 &= x_4,\\
\dot{x}_3 &= \frac{K_m}{m}\left(u_1\psi_{1\alpha} + u_2\psi_{1\beta}\right) - \frac{k_s}{m}x_1,\\
\dot{x}_4 &= \frac{K_m}{m}\left(u_2\psi_{1\alpha} - u_1\psi_{1\beta}\right) - \frac{k_s}{m}x_2 - g.
\end{aligned} \tag{24}$$

Taking the derivative of the output function until each component in $Y_q = ({y_1}^{\alpha 1}, \ldots, {y_q}^{\alpha q})$ include input u explicit.

$$\begin{aligned}
\dot{y}_1 &= x_3,\\
\ddot{y}_1 &= \frac{K_m}{m}\left(u_1\psi_{1\alpha} + u_2\psi_{1\beta}\right) - \frac{k_s}{m}x_1,\\
\dot{y}_2 &= x_4,\\
\ddot{y}_2 &= \frac{K_m}{m}\left(u_2\psi_{1\alpha} - u_1\psi_{1\beta}\right) - \frac{k_s}{m}x_2 - g.
\end{aligned} \tag{25}$$

The Jacobi matrix of the input u can be expressed as

$$A = \begin{bmatrix} \dfrac{\partial \ddot{y}_1}{\partial u_1} & \dfrac{\partial \ddot{y}_1}{\partial u_2} \\ \dfrac{\partial \ddot{y}_2}{\partial u_1} & \dfrac{\partial \ddot{y}_2}{\partial u_2} \end{bmatrix} = \frac{K_m}{m}\begin{bmatrix} \psi_{1\alpha} & \psi_{1\beta} \\ -\psi_{1\beta} & \psi_{1\alpha} \end{bmatrix}. \tag{26}$$

Because $\mathrm{Det}\, A = K_m({\psi_{1\alpha}}^2 + {\psi_{1\beta}}^2)/m \neq 0$, according to Theorem 1, the relative order of the system is $\alpha = (\alpha_1, a_2)^T = (2, 2)^T$, $\alpha_1 + a_2 = 4 = n$, so the system is reversible.

Assuming $\ddot{Y} = \begin{bmatrix} \ddot{y}_1 & \ddot{y}_2 \end{bmatrix}^T = \begin{bmatrix} \phi_1 & \phi_2 \end{bmatrix}^T$, (25) can be calculated as

$$\begin{aligned}
u_1 &= \frac{m}{K_m\left(\psi_{1\alpha}^2 + \psi_{1\beta}^2\right)}\left(\psi_{1\alpha}\phi_1 - \psi_{1\beta}\phi_2 + \frac{k_s}{m}x_1\psi_{1\alpha}\right.\\
&\quad \left. - \frac{k_s}{m}x_2\psi_{1\beta} - g\psi_{1\beta}\right),\\
u_2 &= \frac{m}{K_m\left(\psi_{1\alpha}^2 + \psi_{1\beta}^2\right)}\left(\psi_{1\beta}\phi_1 + \psi_{1\alpha}\phi_2 + \frac{k_s}{m}x_1\psi_{1\beta}\right.\\
&\quad \left. + \frac{k_s}{m}x_2\psi_{1\alpha} + g\psi_{1\alpha}\right).
\end{aligned} \tag{27}$$

In order to realize closed-loop displacement control and improve the performance of anti-interference, SMVS is introduced into the inverse system. The sliding mode switching surface of the sliding mode controller is defined as follows:

$$S_3 = c_1\left(x^* - x\right) + \dot{x}^* - \dot{x},$$

$$S_4 = c_2\left(y^* - y\right) + \dot{y}^* - \dot{y}, \tag{28}$$

where x^* and y^* are the given displacement of x and y direction, x and y are the measured displacement, and c_1 and c_2 are constants.

Exponential reaching law is adopted in this paper and the expression is as follows:

$$\begin{aligned}
\dot{S}_3 &= -\varepsilon_3 \mathrm{sgn}\left(S_3\right) - K_3 S_3,\\
\dot{S}_4 &= -\varepsilon_4 \mathrm{sgn}\left(S_4\right) - K_4 S_4.
\end{aligned} \tag{29}$$

According to (14)-(15), the sliding mode controller is stable. It can be obtained by (28)-(29) that

$$\begin{aligned}
\ddot{x} = \phi_1 &= c_1\left(\dot{x}^* - \dot{x}\right) + \ddot{x}^* + \varepsilon_3 \mathrm{sgn}\left(S_3\right) + K_3 S_3,\\
\ddot{y} = \phi_1 &= c_1\left(\dot{y}^* - \dot{y}\right) + \ddot{y}^* + \varepsilon_4 \mathrm{sgn}\left(S_4\right) + K_4 S_4.
\end{aligned} \tag{30}$$

Torque winding and suspension winding of the BIM are coupled by air gap flux of torque winding, and torque winding can be obtained by torque winding stator flux subtracting stator leakage inductance.

$$\begin{aligned}
\psi_{1\alpha} &= \psi_{1s\alpha} - L_{1sl} i_{1s\alpha},\\
\psi_{1\beta} &= \psi_{1s\beta} - L_{1sl} i_{1s\beta}.
\end{aligned} \tag{31}$$

It can be known from (3) that the stator flux identification in the DTC has the pure integral part. The initial value of integration, the accumulated error, and other factors will make the flux identification inaccurate. Therefore, the traditional suspension force control method cannot meet the requirements of the stable suspension of the BIM. Because of the introduction of SMVS to the suspension force control, the robustness of the controller is improved, the dependence of the accuracy of stator flux estimation is reduced, and the performance of stator stable suspension is improved.

Through the separate control of torque and suspension force, the SMVS-DTC system of the BIM can be constructed, and the structure diagram of the system is showed as Figure 1.

The control block diagram of the BIM includes two parts: torque winding control part and suspension winding control part. In torque winding control part, the voltage and current of the stator are obtained by the coordinate transformation, and then the estimated value of the stator flux is calculated by the stator flux calculation block. The given value of the torque is obtained by the speed regulator, and the estimation value of torque is calculated by torque calculation block. The torque error signal is obtained by given value and the estimation value of torque, and then the voltage control signal of inverter is obtained by SMVS-DTC block. In suspension winding control part, through the SMVS block, the component of levitation force can be calculated by position error signal. The air gap flux is calculated by the stator flux of torque winding; through the inverse system block, the stator current of suspension winding can be calculated by the component of levitation force and the air gap flux, so as to realize radial stable suspension of the rotor.

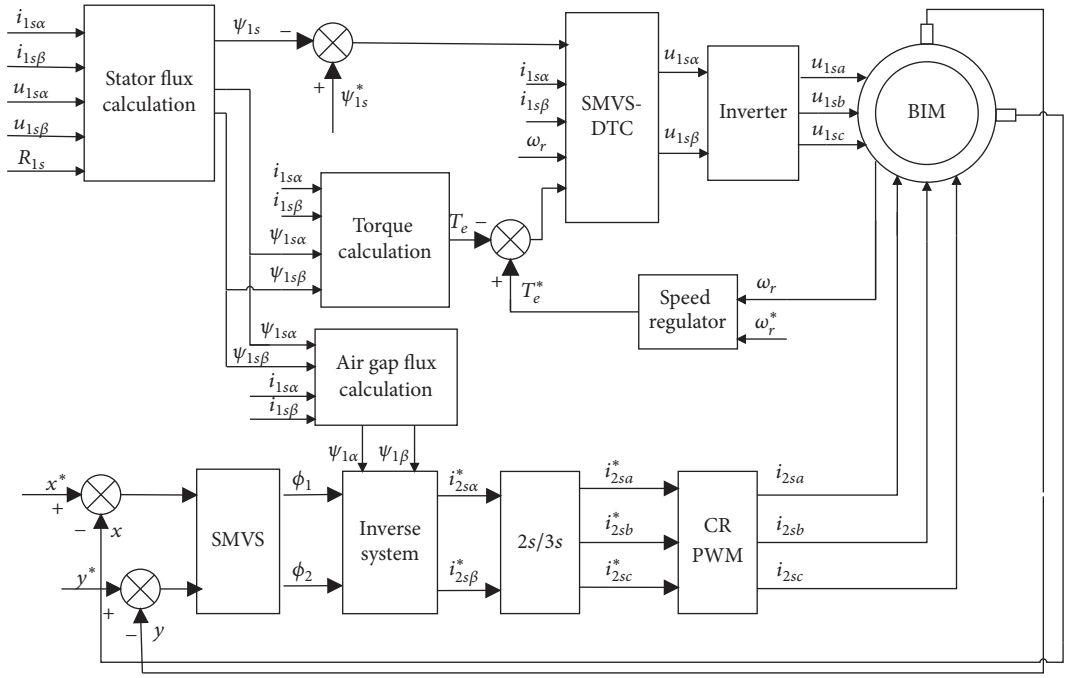

Figure 1: The structure diagram of the BIM SMVS-DTC system.

Table 1: Parameters of the BIM.

Motor parameters	Torque winding	Suspension winding
P (W)	1500	500
n (r/min)	6000	6000
R_s (Ω)	2.01	1.03
R_r (Ω)	11.48	0.075
L_m (H)	0.15856	0.00932
L_{1sl} (H)	0.00454	0.00267
L_{1rl} (H)	0.00922	0.00542
J (kg·m^2)	0.00769	0.00769
m (kg)	2.85	2.85
p	1	2

4. Simulation and Experimental Study of the BIM SMVS-DTC and Suspension Force Control System

4.1. Results and Analysis of Simulation. In order to verify the feasibility of the control method, the simulation model of the BIM SMVS-DTC and suspension force control system is established. The simulation results of SMVS-DTC control method proposed and the traditional DTC control method are compared and analyzed. The simulation parameters are in Table 1.

The simulation parameters are as follows: $\varepsilon_1 = \varepsilon_2 = 0.03$, $K_1 = K_2 = 1500$, $\varepsilon_3 = \varepsilon_4 = 0.01$, and $K_3 = K_4 = 3000$. The given speed is 6000 r/min, and the simulation time is 0.6 seconds. The load torque is added to 2 N·m at t = 0.3 s. To verify the superiority of the proposed method, SMVS-DTC with SMVS suspension force control method and the traditional DTC with traditional suspension force control method are compared and analyzed by simulation. The simulation results are in Figures 2, 3, and 4.

The stator flux trajectory, torque response, and speed response are showed in Figures 2, 3, and 4, respectively. It can be seen from Figure 2(a) that the amplitude of stator flux oscillations is large and the dynamic response is not good by traditional DTC method. From Figure 2(b) we can see that the amplitude of stator flux oscillations is smaller by SMVS-DTC method. Compared with Figures 3(a) and 3(b), we can see that the torque ripple of SMVS-DTC is reduced greatly than traditional DTC. And the dynamic performance of the motor is also improved when the motor is started. When t = 0.3 s the load torque is added. The transition time of the proposed method is reduced. It can be found in Figure 3(b) that there is chattering at steady state due to the sliding mode variable structure control and it can not be avoided, but the chattering is small, which does not affect the stable operation of the motor. From Figure 4, it can be found that the speed rise time has been reduced, and the dynamic response has been improved when using SMVS-DTC method compared to traditional DTC method. In addition, when the load is added, the speed fluctuation is obviously reduced when using SMVS-DTC method.

The simulation results of the rotor motion trajectory and rotor radial displacement by traditional suspension force control method and the proposed method are showed in Figures 5 and 6, respectively. We can see that the proposed method can effectively reduce the radial displacement of the rotor and the displacement fluctuation time, which can realize stable suspension operation of the BIM. In order to verify the performance of antidisturbance of the suspension force control method, the given radial displacement was set

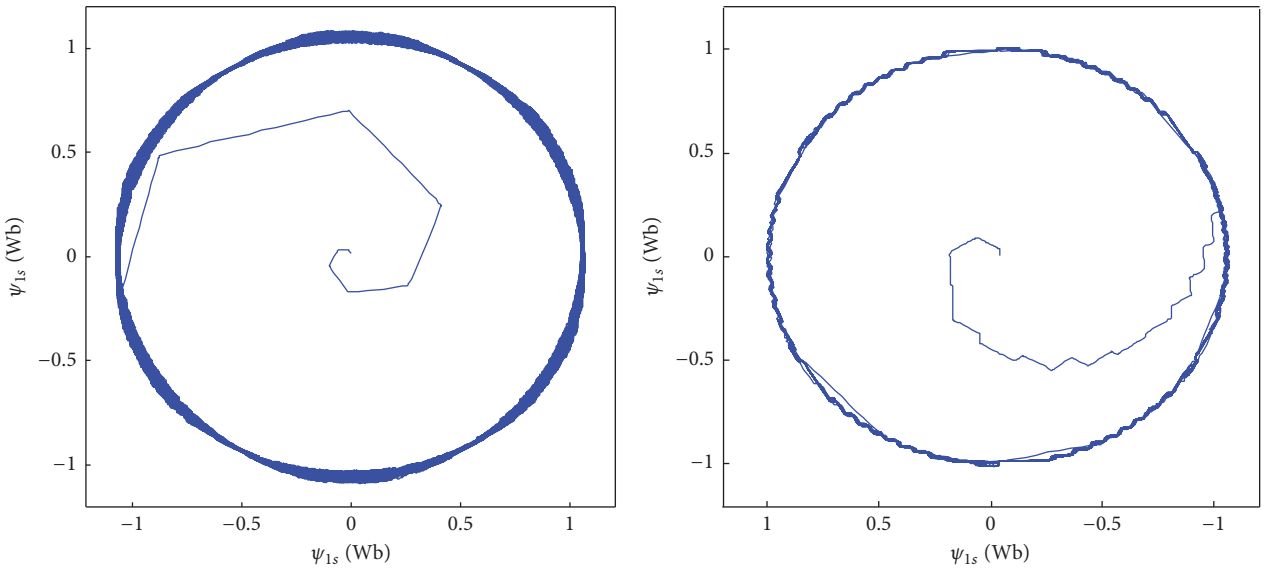

(a) DTC (b) SMVS-DTC

Figure 2: Trajectory of stator flux.

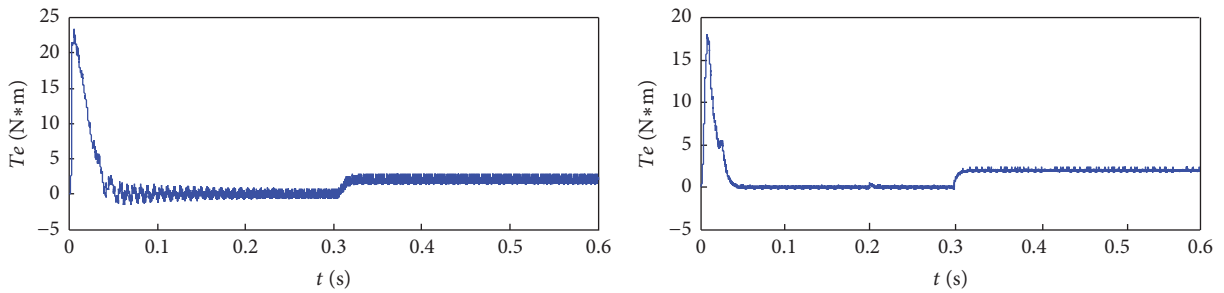

(a) DTC (b) SMVS-DTC

Figure 3: Torque response.

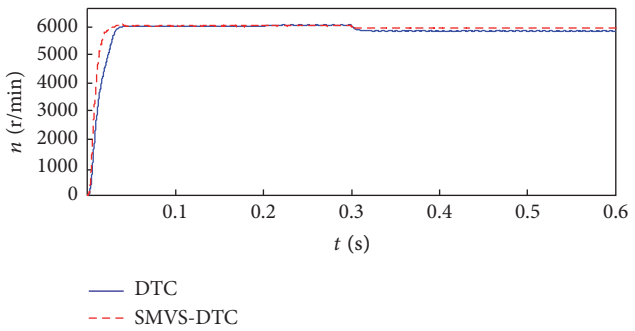

Figure 4: Speed response.

to 0.05 mm when $t = 0.3$, and the simulation waveforms are shown in Figure 7.

As can be seen from the figure, the radial displacement fluctuation is only 0.015 mm, when the given displacement suddenly changed, and the fluctuation time is less than 0.05 seconds, so it has good performance of robustness.

4.2. Results and Analysis of Experiment. In order to verify the effect of the proposed method, experimental research on the prototype of the BIM has been carried out. We analyzed and compared this method with the traditional DTC method. The TI company's 32-bit fixed point DSP chip F2812 is used as the control chip of the control system. The EVA and EVB on this chip can produce six complementary PWM waveforms; therefore, the torque winding and suspension winding of the BIM can be independently controlled. The experimental parameters are similar to the simulation parameters, and rotor speed is set to 2000 r/min, started with no-load, and then the load torque of 2 N·m is added to the motor. The torque responses of these two kinds of DTC methods are compared with the experimental results. The experimental block diagram of the control system is shown in Figure 8 and the experimental results are shown in Figures 9 and 10.

The experimental block diagram of the control system includes two parts: torque winding control part and suspension winding control part. In torque winding control part, the speed signal is obtained by the photoelectric encoder and the DSP (Digital Signal Processor) as the control chip

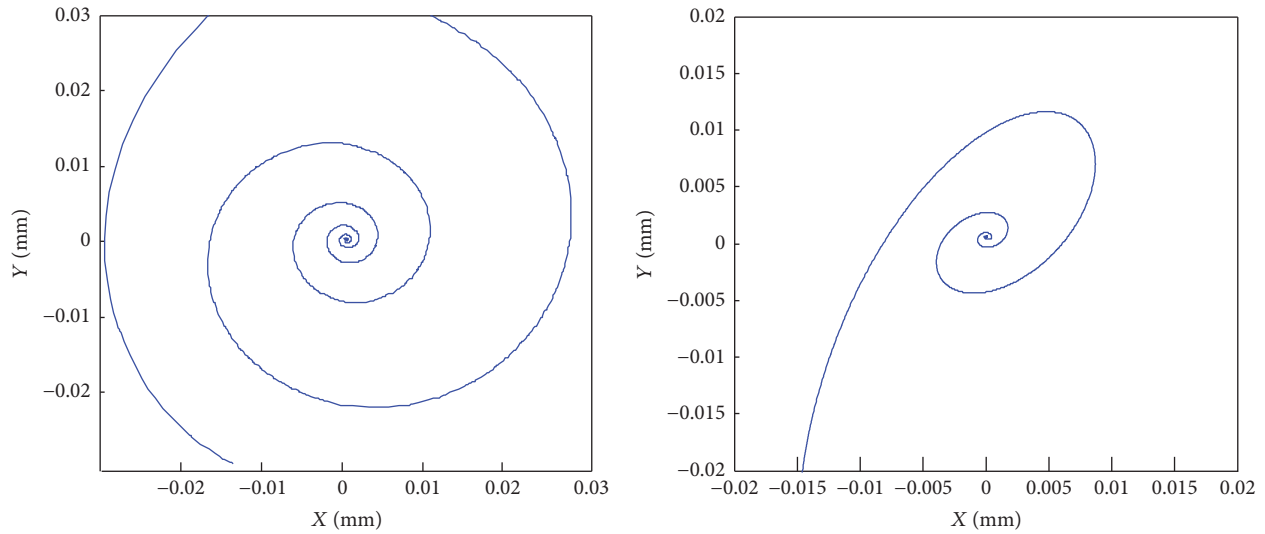

(a) DTC (b) SMVS-DTC

Figure 5: Rotor trajectory.

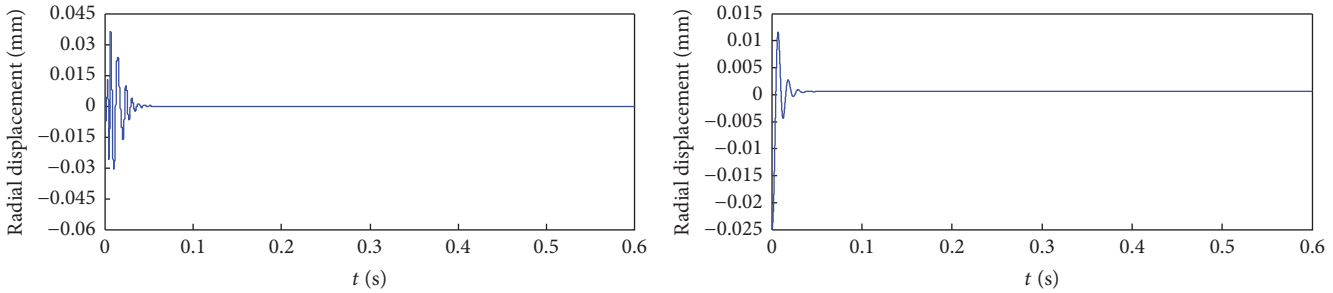

(a) DTC (b) SMVS-DTC

Figure 6: Rotor radial displacement.

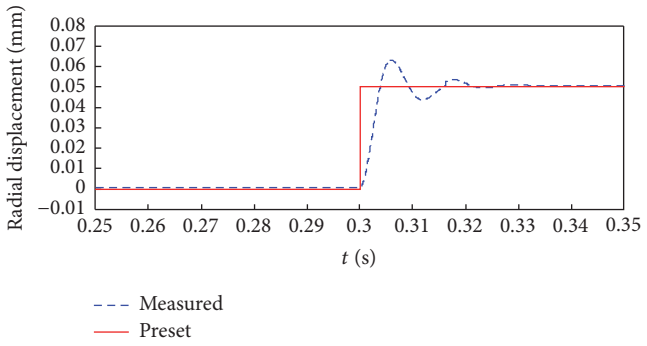

Figure 7: Rotor radial displacement.

of the control system to achieve the SMVS-DTC control. The sample of busbar current and voltage was achieved by the current and voltage sensor. The PWM signal output by DSP was put into IPM (Intelligent Power Module). In suspension winding control part, the radial displacement signal of the suspension winding is obtained by the position sensor, and this signal was put into DSP to realize the closed-loop control of radial displacement. The power drive part of the suspension winding is the same as the torque winding.

Figure 9 is the displacement response of the rotor with SMVS suspension force control method based on inverse system. Figure 10 is the speed and torque response of traditional DTC and SMVS-DTC methods. Figure 9 shows that the rotor displacement in x and y direction is small with the suspension force control method, and it can realize the motor stable suspension operation. We can see from Figure 10(a) that the torque ripple is relatively large when the motor operates with no load and with load, and the torque ripple is large and the dynamic performance is not good when the load is suddenly added; at the same time, the rotor speed is significantly fluctuated. In addition, the BIM is vibrated when the motor starts, accompanied by a sharp noise. It can be known from Figures 10(a) and 10(b) that the torque ripple can be reduced effectively by the proposed method, the torque transition process is faster, and the speed is not fluctuated obviously when the load is suddenly added. The operation noise of experimental prototype is reduced and the starting process is stable with no violent vibration.

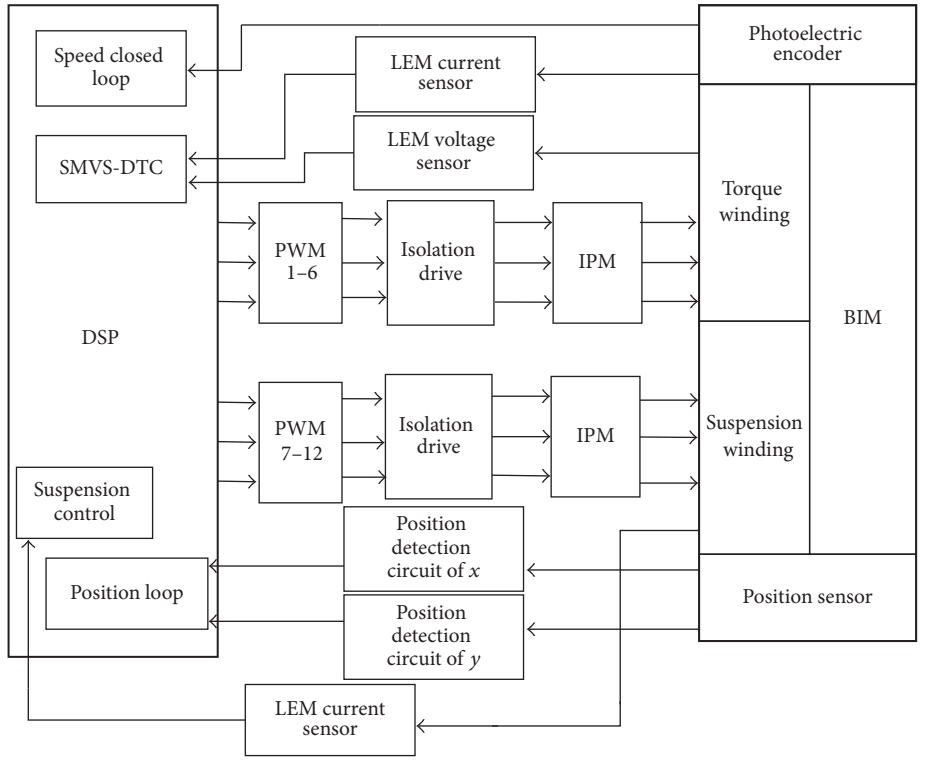

FIGURE 8: The experiment block diagram of the control system.

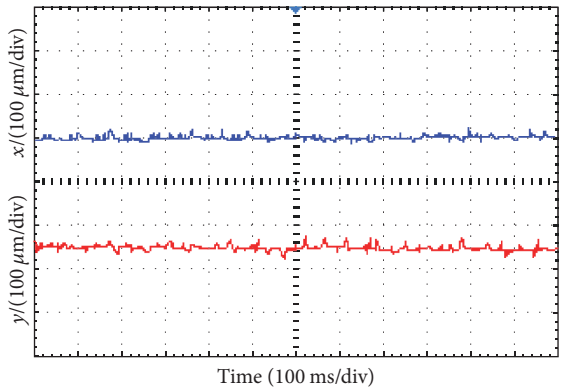

FIGURE 9: Rotor radial displacement.

5. Conclusion

Aimed at the problems of the large torque ripple and unstable suspension performance in traditional DTC and suspension force control of the BIM, the traditional method is improved in this paper and the DTC and suspension force control method based on SMVS are proposed. The performance of torque control and suspension force control of the BIM is better with the proposed method. From the simulation and experiment results of the control system of the BIM based on the traditional DTC and SMVS-DTC, we can draw the following conclusions:

(1) The torque ripple can be reduced effectively and the dynamic performance and the anti-interference ability are improved by SMVS-DTC method.

(2) The SMVS suspension force control method not only reduced the rotor radial displacement fluctuation and fluctuation time but also realized the motor stable suspension operation.

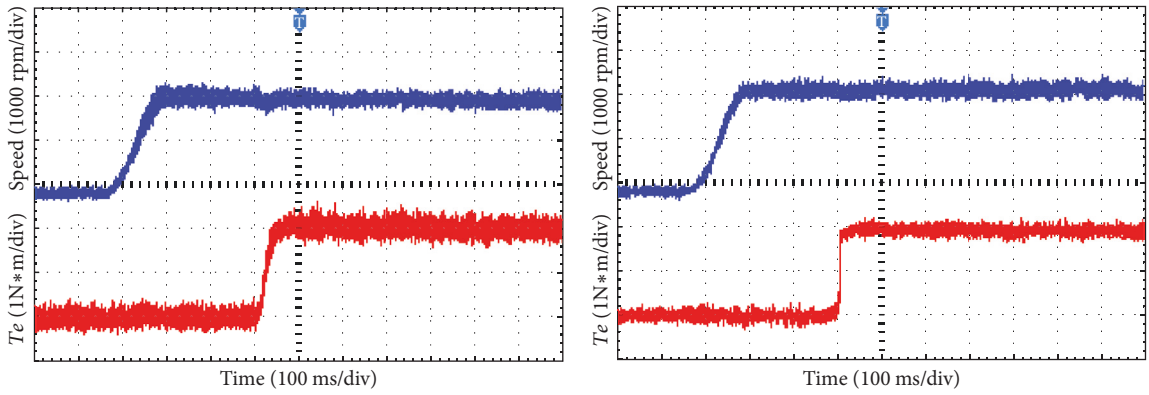

(a) DTC (b) SMVS-DTC

Figure 10: Speed and torque response.

Conflicts of Interest

The authors declare no conflicts of interest.

Acknowledgments

This work was supported by the National Natural Science Foundation of China under Projects 51305170 and 51475214, the Natural Science Foundation of Jiangsu Province of China under Projects BK20141301 and BK20170071, the China Postdoctoral Science Foundation under Projects 2016M601726 and 2015T80508, the Six Categories Talent Peak of Jiangsu Province under Projects 2015-XNYQC-003 and 2014-ZBZZ-017, Zhenjiang Key Research and Development Project under Project GY2016003, the "333 project" of Jiangsu Province under Project BRA2017441, and the Priority Academic Program Development of Jiangsu Higher Education Institutions (PAPD).

References

[1] X. Sun, L. Chen, and Z. Yang, "Overview of bearingless permanent-magnet synchronous motors," *IEEE Transactions on Industrial Electronics*, vol. 60, no. 12, pp. 5528–5538, 2013.

[2] X. Sun, L. Chen, H. Jiang, Z. Yang, J. Chen, and W. Zhang, "High-performance control for a bearingless permanent-magnet synchronous motor using neural network inverse scheme plus internal model controllers," *IEEE Transactions on Industrial Electronics*, vol. 63, no. 6, pp. 3479–3488, 2016.

[3] Z. Yang, L. Wan, X. Sun, L. Chen, and Z. Chen, "Sliding Mode Control for Bearingless Induction Motor Based on a Novel Load Torque Observer," *Journal of Sensors*, vol. 2016, Article ID 8567429, 2016.

[4] Z. Wang and X. Liu, "An improved rotor flux oriented control system of bearingless induction motors," in *Proceedings of the Chinese Control and Decision Conference (CCDC '10)*, pp. 2733–2737, May 2010.

[5] X. Wang, Z. Deng, and Y. Yan, "The nonlinear decoupling control of the bearingless induction motors based on the air-gap flux orientation," *Transactions of China Electrotechnical Society*, vol. 6, p. 4, 2002.

[6] Y. X. Sun, C. S. Xu, and H. Q. Zhu, "A Three-Level DTC System Based on Virtual Space Vector Modulation for Bearingless Permanent Magnet Synchronous Motor," *Applied Mechanics and Materials*, vol. 703, pp. 356–359, 2014.

[7] H. Zhu and Y. Gu, "Direct torque control and direct suspension force control of bearingless permanent magnetic slice motor," *Paiguan Jixie Gongcheng Xuebao/Journal of Drainage and Irrigation Machinery Engineering*, vol. 6, p. 16, 2015.

[8] Y. Wang, Z. Deng, and X. Wang, "Direct torque control of bearingless induction motor," in *Proceedings of the CSEE*, vol. 28, pp. 80–84, 2008.

[9] X. Liu, H. Chen, and J. Zhou, "SVM-DTC System for bearingless induction motor based on discrete time deadbeat," *Bearing*, vol. 3, 2012.

[10] Y. Liao, X. Feng, and Z. Wang, "Induction Motor Direct Torque Control Based on Stator Flux Sliding Mode Observer and Space Vector Pulse Width Modulation," in *Proceedings of the CSEE*, vol. 18, p. 12, 2012.

[11] Y. Liu, L. M. Shi, and L. Zhao, "Direct torque control of asynchronous motor based on hybrid flux observer," *Transactions of China Electrotechnical Sosiety*, vol. 30, no. 10, pp. 157–163, 2015.

[12] B. Wang, Y. Wang, W. Guo, and Z. Wang, "Deadbeat direct torque control of permanent magnet synchronous motor based on reduced order stator flux observer," *Diangong Jishu Xuebao/Transactions of China Electrotechnical Society*, vol. 29, no. 3, pp. 160–171, 2014.

[13] X. Sun, L. Chen, Z. Yang, and H. Zhu, "Speed-sensorless vector control of a bearingless induction motor with artificial neural network inverse speed observer," *IEEE/ASME Transactions on Mechatronics*, vol. 18, no. 4, pp. 1357–1366, 2013.

[14] Y. Xu, Y. Lei, L. Ma, and D. Sha, "A novel direct torque control of permanent magnet synchronous motors based on backstepping control," *Diangong Jishu Xuebao/Transactions of China Electrotechnical Society*, vol. 30, no. 10, pp. 83–89, 2015.

[15] S. Lv, L. Shuai, M. Hui, and Q. Dong, "Direct torque control for permanent magnet synchronous motor with optimal duty cycle control," *Diangong Jishu Xuebao/Transactions of China Electrotechnical Society*, vol. 30, pp. 35–42, 2015.

[16] J. Huang, Q. Xu, X. Shi, L. Cui, and Z. Xiang, "Direct torque control of PMSM based on fractional order sliding mode variable structure and space vector pulse width modulation," in

Proceedings of the 33rd Chinese Control Conference (CCC '14), pp. 8097–8101, July 2014.

[17] H. Li and H. Zhu, "Bearingless motor's radial suspension force control based on virtual winding current analysis," in *Proceedings of the 17th International Conference on Electrical Machines and Systems (ICEMS '14)*, pp. 2141–2146, October 2014.

[18] Y. Shtessel, C. Edwards, L. Fridman, and A. Levant, *Sliding Mode Control and Observation*, Birkhäuser, Springer, New York, NY, USA, 2014.

[19] C. Lascu and F. Blaabjerg, "Super-twisting sliding mode direct torque contol of induction machine drives," in *Proceedings of the Energy Conversion Congress and Exposition (ECCE '14)*, pp. 5116–5122, 2014.

[20] B.-Z. Guo and F.-F. Jin, "Sliding mode and active disturbance rejection control to stabilization of one-dimensional anti-stable wave equations subject to disturbance in boundary input," *Institute of Electrical and Electronics Engineers. Transactions on Automatic Control*, vol. 58, no. 5, pp. 1269–1274, 2013.

[21] J.-J. Liu and J.-M. Wang, "Boundary stabilization of a cascade of ODE-wave systems subject to boundary control matched disturbance," *International Journal of Robust and Nonlinear Control*, vol. 27, no. 2, pp. 252–280, 2017.

[22] A. Wang, X. Jia, and S. Dong, "A new exponential reaching law of sliding mode control to improve performance of permanent magnet synchronous motor," *IEEE Transactions on Magnetics*, vol. 49, no. 5, pp. 2409–2412, 2013.

[23] Z. Yang, D. Dong, H. Gao, X. Sun, R. Fan, and H. Zhu, "Rotor mass eccentricity vibration compensation control in bearingless induction motor," *Advances in Mechanical Engineering*, vol. 7, no. 1, Article ID 168428, 2015.

[24] X. Sun, B. Su, L. Chen, Z. Yang, X. Xu, and Z. Shi, "Precise control of a four degree-of-freedom permanent magnet biased active magnetic bearing system in a magnetically suspended direct-driven spindle using neural network inverse scheme," *Mechanical Systems and Signal Processing*, vol. 88, pp. 36–48, 2017.

[25] X. Sun, Z. Shi, L. Chen, and Z. Yang, "Internal model control for a bearingless permanent magnet synchronous motor based on inverse system method," *IEEE Transactions on Energy Conversion*, vol. 31, no. 4, pp. 1539–1548, 2016.